Milling of maraging steel components produced by selective laser melting

Alessandro Fortunato[a], Amarildo Lulaj[a], Shreyes Melkote[b], Erica Liverani[a], Alessandro Ascari[a], Domenico Umbrello[c].

[a] *Department of Industrial Engineering, Università di Bologna, Bologna, Italy*

[b] *George W. Woodruff School of Mechanical Engineering, Georgia Institute of Technology, Atlanta, GA 30332, USA*

[c] *Department of Mechanical, Energy and Management Engineering, University of Calabria, Rende CS 87036, Italy*

This paper presents an experimental study of milling operations performed on 18Ni(300) maraging steel components produced by selective laser melting (SLM). The aim was to identify the optimum manufacturing process chain to obtain the best properties of finished 18Ni(300) molds produced by a combination of additive and subtractive manufacturing methods. The SLM process variables taken into consideration were the build direction and post-build heat treatment, while cutting speed was considered as the only process variable for the milling phase. Surface roughness and hardness, cutting forces and tool wear were considered for the evaluation of the optimal manufacturing process parameters.

Milling, Mold, Selective laser melting (SLM).

---

1. Introduction

Maraging steels are a class of ultra-high strength steels with good mechanical properties obtained by means of precipitation strengthening. Gonçalves dos Reis et al. (2015) investigates the microstructure of 300 Maraging steel and its correlation with creep behavior at high temperature and demonstrates a good behavior up to 550°C. The microstructures impart high yield strength, good resistance to crack propagation and thermal fatigue and machinability up to these temperatures. These properties have promoted the use of maraging steels for the fabrication of molds for plastic injection molding, and aluminum and zinc alloy die-casting. Jhavar et al. (2013) added Maraging steels in their list of suitable filler materials which successfully repair of mold/die. A significant limitation of mold fabrication using conventional technology is the development of high thermo-mechanical stresses due to difficulty in creating internal cooling channels in the mold. Conversely, additive

processes are more effective for creating cooling channels, thereby enhancing the life of the mold as clearly described by Hölker and Tekkaya (2016). In particular, Altan et al. (2001) indicated the powder bed processes (like SLM) as the most suitable processes for the internal channel fabrication, due to powder supports of overhanging volumes.

Furthermore, Thompson et al. (2016) showed that the SLM process allows easy customization of the mold shape and of the final product.

Becker and Dimitrov (2016) demonstrated that it is possible to find SLM process parameters that yield suitable component properties, while Kempen et al. (2011) showed the beneficial effects of heat treatment.

However, several challenges must be overcome before using SLM for mold manufacturing, some of which include:

- Identifying the necessary finishing operations to achieve good surface finish following the SLM process.
- Defining the optimum manufacturing process chain, taking into account heat treatment and tool wear.

In this paper, the optimum SLM parameters for maraging steel powder capable of producing high strength components were determined by means of density measurements and tensile tests. These parameters were then used to fabricate samples for finishing by means of face milling with ceramic inserts. In order to define the optimum manufacturing process chain, three different heat treatments were performed on the samples, and, together with the SLM process parameters and the cutting speed, their influence on tool wear, cutting forces, surface roughness, and microstructures were investigated.

2. SLM Process

The powders were provided by PRAXAIR with a chemical composition equivalent to 18Ni(300) . The spherical shaped powders (15-45 μm size range) were produced by vacuum-assisted argon atomization.

A preliminary experimental campaign was carried out to determine the optimal SLM process parameters for producing SLM samples having maximum density and the best mechanical properties. The samples were characterized using tensile tests and density measurements according to the ISO 6892-1 standard. The density of each sample was measured by the Archimedes' method and the tensile tests were performed on a hydraulic tensile testing machine equipped with a 100 kN load cell. All samples were fabricated in a SISMA MYSINT100 SLM machine with a maximum laser power of 150 W and a focused spot diameter of 50 μm. The experimental campaign is summarized in Table 1; the layer thickness and the hatch space were kept constant at 30 μm and 60 μm, respectively. All samples were built in the vertical direction.

Table 1 SLM process parameters

Power [W]	Scan rate [mm/s]	Fluence [J/mm^3]
100	500; 700; 900	62 - 111
120		74 - 133
150		93 - 167

The SLM samples were fabricated in a nitrogen environment with 0.3% volume of residual oxygen. The scanning strategy consisted of subdividing each layer into a chessboard, where each square block was melted using a meandering laser path. A detailed explanation of the scanning strategy is presented by Liverani et al. (2016) in their previous work. The resulting mechanical properties and densities are reported in Figure 1. Increasing the density of the samples (by increasing the laser fluence) increased the strength and elongation of the tensile samples.

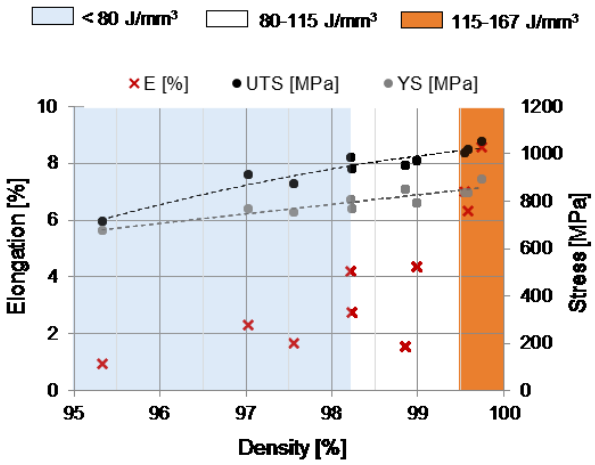

Figure 1. SLM process optimization for maraging steels.

Based on these results, the following optimal SLM process build parameters were established: laser power of 150 W and a scanning speed of 500 mm/s, resulting in a fluence of 167 J/mm^3. Sixteen (16) SLM samples with geometry shown in Figure 2 were fabricated using the build parameters for face milling tests. Following sample fabrication, four (4) of the SLM samples were partially heat treated (PT) using a solutionizing treatment (heating at 815 °C for 1 hour followed by air cooling), four (4) samples were totally heat treated (TT) using a solutionizing plus ageing (480 °C for 4 hours followed by air cooling) treatment, and the remaining eight (8)

samples were not treated (NT). In order to investigate the influence of SLM build direction, four (4) NT samples were fabricated using a build direction of 90° while another four (4) were built in the 0° direction, see Figure 3.

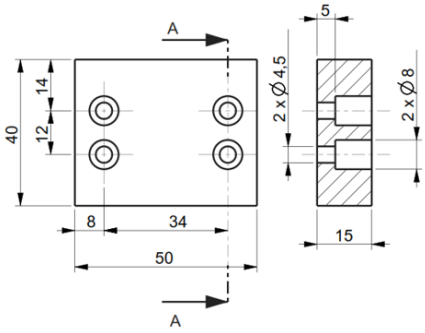

Figure 2. Geometry of the samples for milling tests.

3. Materials and methods

3.1. SLM sample characterization

The following attributes of all SLM samples were initially characterized: microstructure, roughness, and hardness. The roughness was measured in an Olympus LEXT OLS 4000 Confocal Laser Microscope. For each sample, 40 measurements were made on the top surface located between the clearance holes, see Figure 3. The hardness of each sample was measured at 40 locations using a Rockwell C test, as shown in Figure 3.

In order to minimize the influence of the as-built surface irregularity, the SLM surfaces were ground very lightly prior to the hardness measurements.

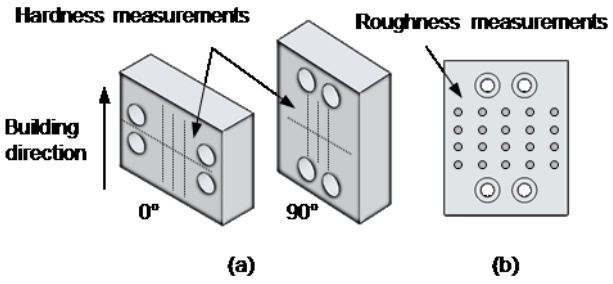

Figure 3. Procedure for hardness and roughness measurements.

3.2. Face milling tests

Face milling experiments were performed on the 16 SLM samples. The test setup is shown schematically in Figure 4. Note that the cutting forces were measured using a three-component Kistler 9257B dynamometer.

A 50.88 mm diameter face milling cutter (Kennametal KSSR25ORP430C3) with 4 round ceramic inserts (Kennametal RPG43E) were used. The samples were clamped using 4 screws to the mounting plate, which was fixed to the dynamometer. Cutting was performed in one pass with the tool moving in the *y* direction (feed direction).

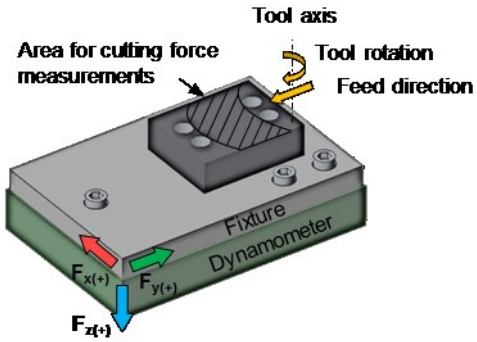

Figure 4. Schematic of the face milling test setup.

All milling tests were carried out at a constant axial depth of cut of 500 µm and a constant feed of 0.08 mm/rev. Two cutting speeds were used: 190 m/min and 380 m/min, which were obtained using spindle speeds of 1189 rpm and 2377 rpm, respectively. These spindle speeds yielded the following feed rates: 95 mm/min and 190 mm/min. Two repetitions of each test combination were carried out. Note that the effect of SLM build orientation on the milling process response was only considered for the untreated (NT) samples since the heat treatment process produces a different microstructure. The labels used to identify the different test results presented in the paper are: ##_AA_XY where ## indicates the build direction, AA refers to the heat treatment condition, X refers to the cutting speed (1=190 m/min; 2=380 m/min), and Y refers to the test repetition number. All milling tests were performed under dry cutting conditions.

4. Results and discussion

4.1. Hardness and microstructures

Figure 5 shows the hardness of the samples before and after milling for all test combinations. It can be seen that the PT samples have a slightly lower hardness than the NT samples, while the TT samples have the highest hardness. It can also be seen that the mean hardness of all samples increases slightly after milling due to the associated plastic deformation. As expected, the differences in the hardness for the two SLM build directions (NT samples) are not significant.

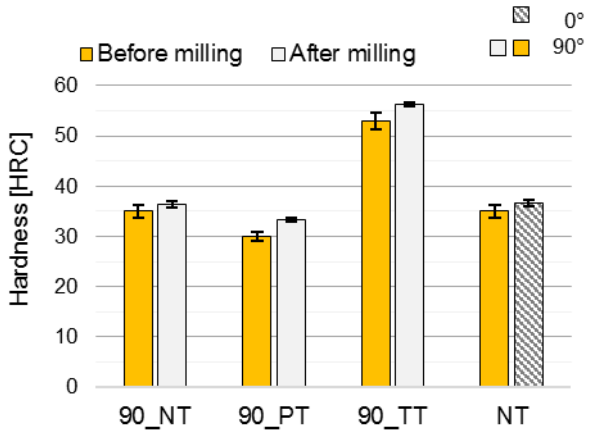

Figure 5: Hardness (HRC) before and after milling.

Figure 6 shows a representative microstructure of the untreated (NT), solutionized (PT), and solutionized and aged (TT) samples. Typical martensitic structures, with and without intermetallic precipitates, are evident in the TT and PT samples in Figure 6(c) and 6(b), respectively, in contrast to the untreated sample microstructure in Figure 6(a).

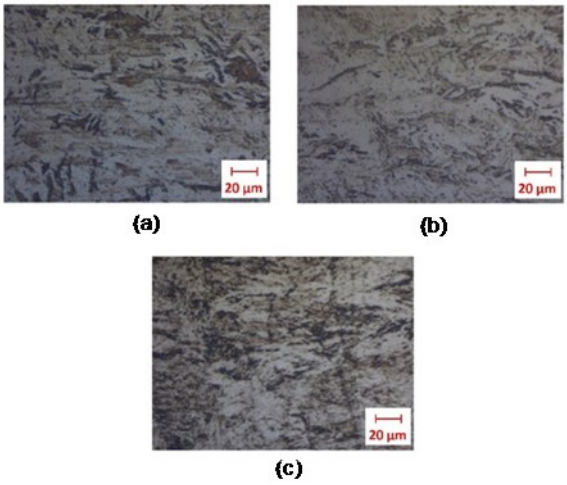

Figure 6. Optical micrographs: a) 90_NT, b) 90_PT, c) 90_TT.

4.2. Cutting forces and tool wear

Cutting forces were acquired during milling of the NT, PT and the TT samples at low and high cutting speeds. The NT sample was also investigated to understand the effect of SLM build direction (0° and 90°) on the milling performance. The force acquisition has been obtained according to Figure 4 which explain the displacement of the tools. For all the considerations regarding cutting forces only the step 2 was taken onto account where

no geometrical discontinuity due to the holes of the screws are presented. An example of force acquisition is presented in Figure 7.

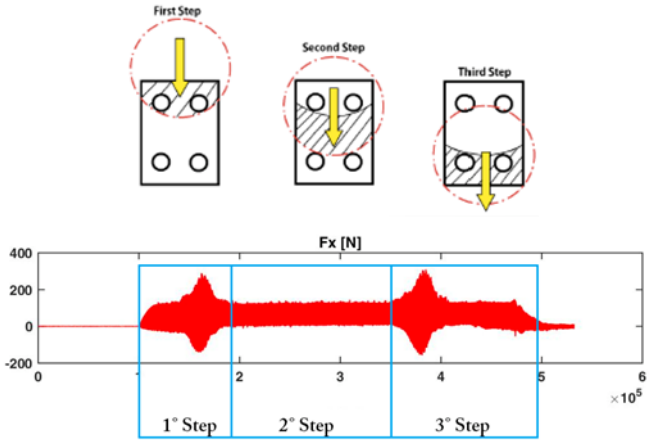

Figure 7. Cutting force acquisition outline

If we consider step 2, according to Figure 8, for cutting speed of 190 m/min, for our 4 cutting inserts tool with an angular distance β=90° and our sample length, we have a working angle 2φ=1.81 rad, a revolution time of the inserts t_2=0.05 sec, a cutting time of every insert t_1=0.014 sec and angle α = 2φ–β = 13.66° where two cutting insert are simultaneously cutting the sample.

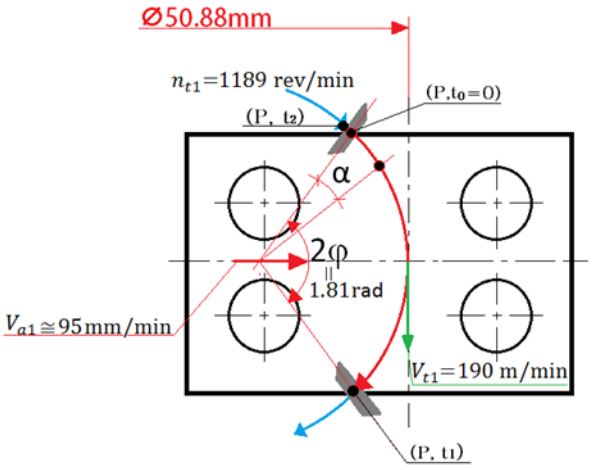

Figure 8. Cutting outline in step 2 for V_t = 190 m/min and V_a = 95 mm/min

Finally, the force acquisition for one tool revolution, in the case of kinematic condition in Figure 8, is reported in Figure 9. For every cutting insert there is a peak force representative of the contact of the second insert (angle α).

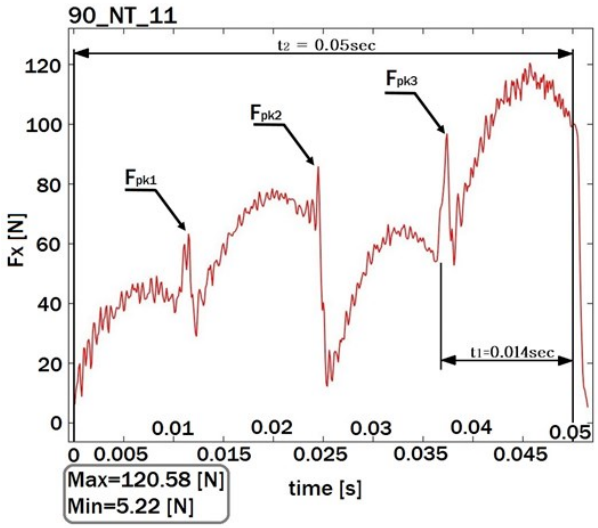

Figure 9. Cutting outline in step 2 for Vt=190 m/min and Va=95 mm/min

Figure 10 summarizes the average cutting force measurements over all the tests, in step 2.

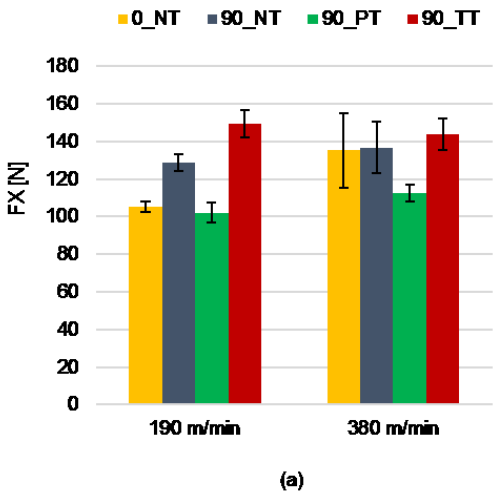

(a)

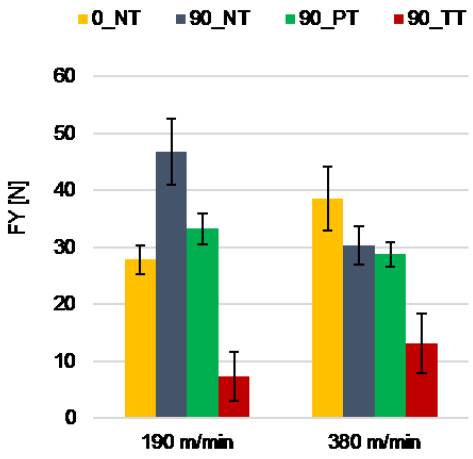

(b)

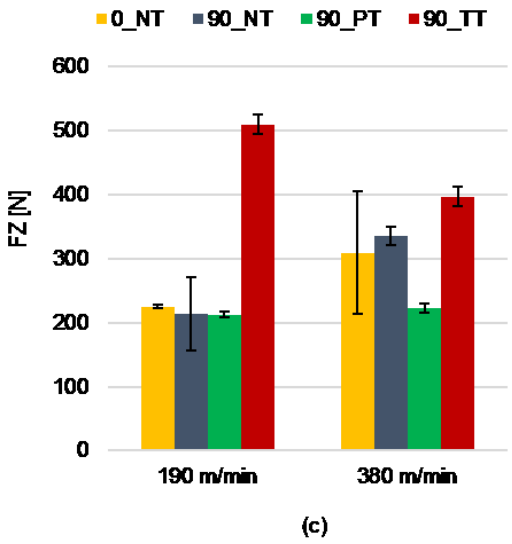

Figure 10. Average resultant cutting forces at as a function of cutting speed heat treatment along the path: (a) transverse force (F_x),(b) axial force (F_z), and (c) feed force (F_y).

An increase in the cutting speed is generally linked to an increase in the cutting temperature and, consequently, a decrease in the cutting forces due to thermal softening. In this work both the average transverse F_x and average axial forces (F_z) for the NT samples increase with increasing cutting speed, while the build direction has minimal effect on the cutting forces at low cutting speed. This trend is due to the higher tool wear, which geometry is reported in Figure 11, observed at the high speed (Figure 12), which affects the geometry of the cutting tool causing the forces to increase. For the PT samples, the force increase is almost negligible due to the low wear. In contrast, the TT samples show the reverse trend since the average transverse F_x and the average axial forces F_z decrease with increasing speed. The reason is related to thermal softening associated with the heat treatment used. In fact, for the solutionized and aged samples (TT), the higher temperature reached at the high cutting speed increases thermal softening during milling.

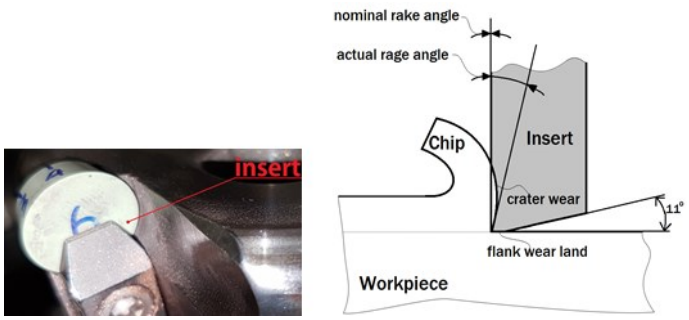

Figure 11. Tool geometry.

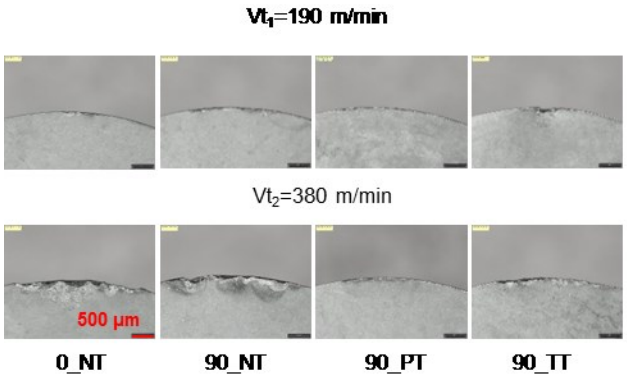

Figure 12. Tool wear for different process combinations.

A more detailed trend of the F_x forces during milling is reported in Figure 13 as a function of the different initial microstructures. In this figure, the maximum transverse force F_x measured along the cutting path is reported, highlighting the combined effect of microstructural transformation, thermal softening, and tool wear. According to Rohrbach ans Schmidt (1190), martensite softening after aging starts above 200 °C, while microstructural transformation starts above the austenite transformation of 800 °C in the NT samples.

The latter effects are highlighted by the different slopes of the force data. The TT samples, going from high to low cutting speeds, exhibit a smaller slope variation, compared to the NT and PT samples, because martensite softening at high cutting speed reduces tool wear and force increase. The two slopes are m=0.95 and m=1.4 for 90_TT_12 and 90_TT_21, respectively. The greatest increase was measured for the NT samples going from low to high cutting speed, with slopes of 0.46 at low speed and 4.4 at high speed. This behavior can be explained by the fact that no significant microstructural modification takes place during cutting, and thermal softening is not sufficient to compensate for tool wear. Finally, the PT samples exhibited average behavior (low cutting speed slope of 0.7 and high cutting speed slope of 1.7) in accordance with the minimum initial hardness of the samples, thermal softening, and consequent minimum tool wear. The PT samples always exhibited the minimum initial F_x The axial force F_z otherwise decreased with increasing cutting speed for all the samples since tool wear affects the feed force only slightly.

Therefore, by increasing the cutting speed, average feed forces F_y always decreases, average axial forces F_z and average transverse forces F_x increase for NT and PT samples and decrease for TT samples.

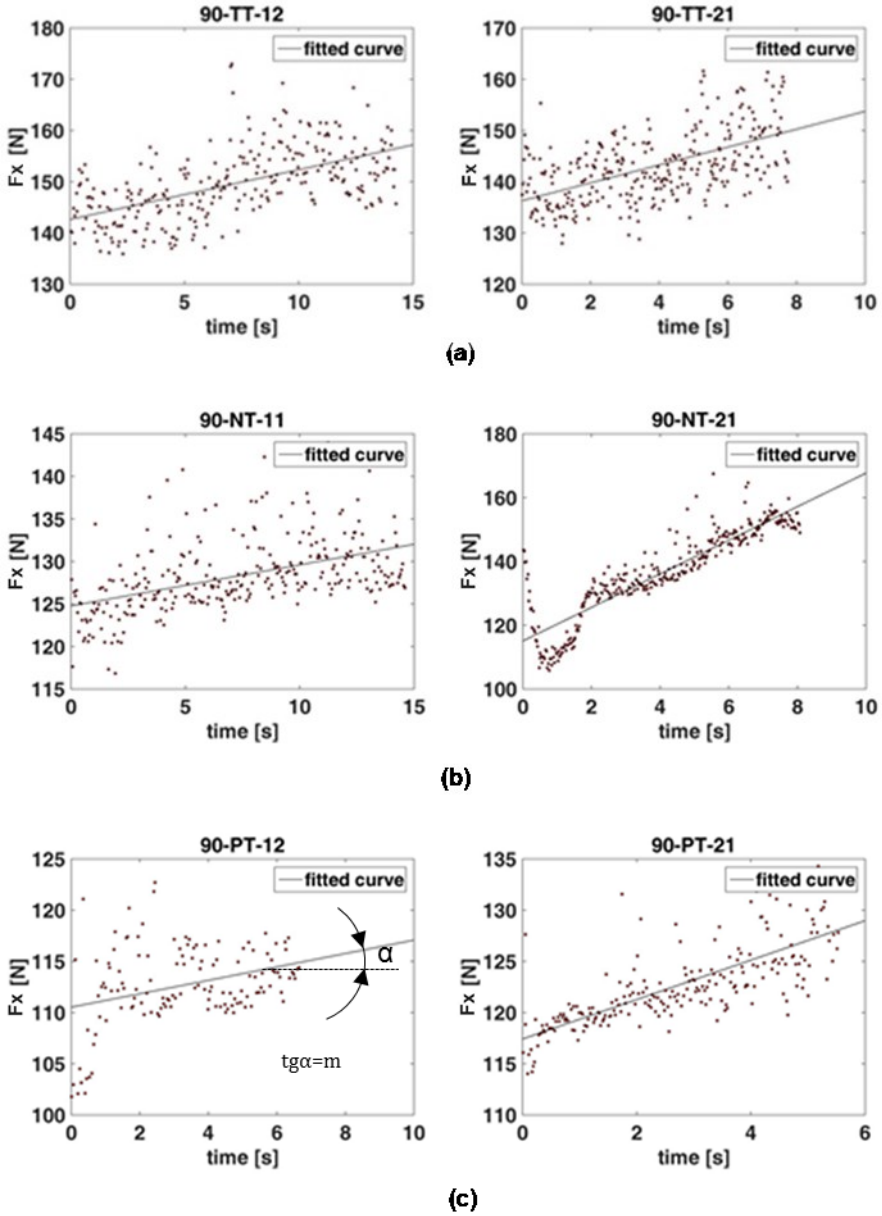

Figure 13. Maximum transverse force F_x along the cutting path for low and high cutting speeds: (a) 90_TT samples, (b) 90_NT samples (c) and 90_PT samples.

4.3. Roughness

Figure 14 shows a typical surface measured by the confocal laser microscope before and after milling. Roughness S_a before milling has an average value of 11,86 μm and standard deviation of 4,9 for 90° build direction samples and S_a = 8,72 m St.dev = 2,62 for 0° samples. As seen in Figure 15, the roughness is greatly improved after milling for every process parameter combination. Analysing Figure 15, the maximum roughness after milling was 0.45 Sa for 90_NT samples at the highest cutting speed. The roughness for the remaining cases are lower and range between 0.175 Sa (90_TT at highest cutting speed) and 0.292 Sa (0_NT at highest

cutting speed). From Figure 15, it is also evident that for the untreated samples, increasing the cutting speed leads to an increase in the average roughness. For both the fully treated (TT) and solution treated (PT) samples, an increase in cutting speed produces a lower average roughness.

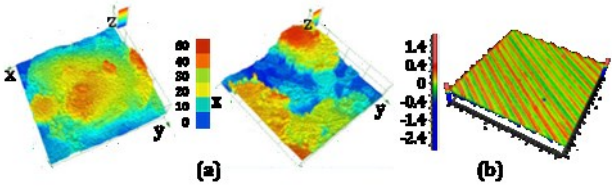

Figure 14. Surface texture maps (a) before and (b) after milling.

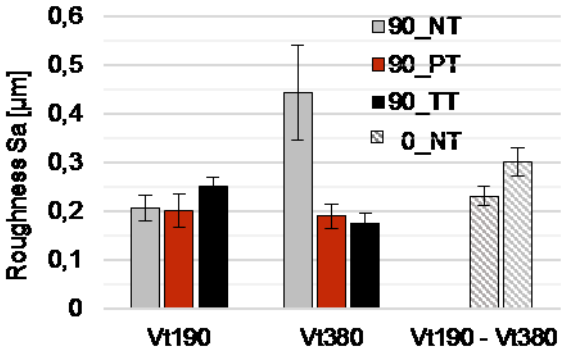

Figure 15. Average surface roughness (Sa) after milling for the different process combinations.

Figure 16 reports the roughness variation along the cutting direction. Going from the entrance to exit of the cut, roughness increases due to tool wear, which is more significant for the untreated samples as seen in Figure 8.

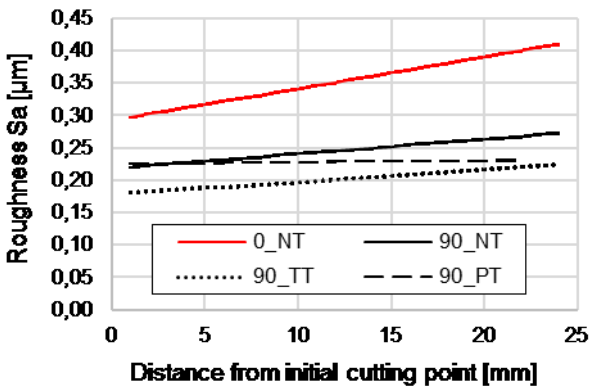

Figure 16. Average surface roughness (Sa) variation during milling for the different SLM samples.

5. Conclusion

This paper reports on the optimum manufacturing process chain for finishing 18Ni300 maraging steel components fabricated by SLM technology. Starting from the results of a preliminary campaign for SLM process parameter optimization, semi-finished SLM samples were fabricated for a cutting campaign performed with a face milling process. The parameters investigated in the cutting campaign were: SLM build direction (0 and 90), post-build heat treatment, and cutting speed. The measured outputs were: surface hardness and roughness, microstructure, cutting forces, and tool wear.

According to the experimental results the following statements can be affirmed:

- The minimum tool wear is observed for the PT samples, while the maximum occurs for the NT samples. Cutting forces increase during milling due to tool wear but the amount of increase depends on the sample; it is maximum for the NT samples, and minimum for the TT samples.
- Increasing the cutting speed improves the surface roughness for the PT and TT samples. The minimum roughness (0.175 Sa) was obtained for the TT samples at the higher cutting speed.
- Very low roughness (below 0.45 μm) was achieved for all the process combinations.

To summarize, the best process chain for the 18Ni(300) maraging mold fabrication is the following:

- SLM manufacturing with P=150 W scanning speed=500 mm/s and fluence=167 J/mm^3 leads to high mechanical property components such as high density and high ultimate tensile stress for the semi-finished part.
- Solution heat treatment and aging leads to the desired martensitic microstructure.
- Finishing by means of milling after heat treatment produces very low roughness, and low tool wear.

References

Altan, T., Lilly, B., Yen, Y.C., 2001. Manufacturing of Dies and Molds. CIRP Annals - Manufacturing Technology. 50 (2), 404-422.

Becker, T. H.; Dimitrov, D., 2016. The achievable mechanical properties of SLM produced Maraging Steel 300 components. Rapid Prototyping Journal. 22 (3), 487-494.

Gonçalves dos Reis, A., Aparecida Pereira Reis, D., Abdalla, A. J., Meijer, J., Otubo, J., 2015. High-temperature creep resistance and effects on the austenite reversion and precipitation of 18 Ni (300) maragings steel. Material Charact. 107, 350-357.

Hölker, R., N., B., Tekkya, A., E., 2016. Advancements in the manufacturing of dies for hot aluminum extrusion with conformal cooling channels. Int J Adv Manuf Technol. 83, 1209-1220.

Jhavar, S., Paul, C., P., Jain, N., K., 2013. Causes of failure and repairing options for dies and molds: A review. Engineering Failure Analysis. 34, 519-535.

Kempen, K.; Yasa, E.; Thijs, L.; Kruth, J.-P.; Van Humbeeck, J., 2011. Microstructure and mechanical properties of Selective Laser Melted 18Ni-300 steel. Physics Procedia. 12, 255-263.

Liverani, E., Fortunato, A., Leardini, A., Belvedere, C., Siegler, S., Ceschini, L., Ascari, A., 2016. Fabrication of Co-Cr-Mo endoprostheticankle devices by means of selective Laser Melting (SLM). Materials & Design. 106, 60-68.

Rohrbach, K., Schmidt, M., 1990, Maraging steels, ASM Handbook - Properties and Selection: Irons Steels and High Performance Alloys, ASM Int, OH, vol.1, pp. 793–800.

Thompson, M., K., Moroni, G., Vaneker, T., Fadel, G., Campbell, R., I., Gibson, I., Bernard, A., Schulz, J., Graf, P., Ahuja, B., Martina, F., 2016. Design for Additive Manufacturing: Trends, opportunities, considerations, and constraints. CIRP Annals - Manufacturing Technology. 65, 737-760.